International Journal of Nanomedicine

Dovepress
Taylor & Francis Group

Open Access Full Text Article

ORIGINAL RESEARCH

Bupivacaine Nanoparticles Inhibit Triple-Negative Breast Tumor Growth by Suppressing the Noradrenergic Nerves in Tumor Microenvironment

Haixuan Wu[1,*], Xiaoyan Huang[1,*], Hui Xu[1,*], Hongmei Yang[1], Zhongqi Liu[1], Fan Liu[2], Fengtao Ji[1], Minghui Cao[1]

[1]Department of Anesthesiology, Sun Yat-Sen Memorial Hospital, Sun Yat-Sen University, Guangzhou, People's Republic of China; [2]Medical Research Center of Shenshan Medical Center, Memorial Hospital of Sun Yat-Sen University, Shanwei, People's Republic of China

*These authors contributed equally to this work

Correspondence: Fengtao Ji; Minghui Cao, Email tqjshmily@139.com; caomh@mail.sysu.edu.cn

Background: Nerves in the tumor microenvironment (TME) promote malignant phenotypes of cancer. Neuron-targeting cancer treatment strategies have garnered significant attention. However, existing pharmacological or surgical methods of denervation can lead to side effects such as pain and respiratory system issues. Targeted delivery of local anesthetics to the TME using nanotechnology to suppress nerves appears to be a promising approach.

Methods: NP-BUP, an acid-responsive nanoparticle encapsulating the local anesthetic bupivacaine, was synthetized using a nano-precipitation method. Immunofluorescence staining was employed to identify the primary types of nerves in breast tumors. In vitro, the impact of the neurotransmitter on the recruitment of macrophages by tumor supernatant is assessed using the transwell assay. ELISA assays and intracellular Ca^{2+} measurement experiments were conducted to evaluate the inhibitory effect of NP-BUP on noradrenergic neurons. In vivo, the impact of NP-BUP on noradrenergic neurons, tumor-associated macrophages (TAMs) infiltration, and tumor growth within the TME were assessed.

Results: The predominant type of neuron within breast tumor tissues was found to be noradrenergic neuron. Noradrenergic neuronal uptake of NP-BUP at pH 6.5 was 2.4 times higher than at pH 7.4. In vitro, NP-BUP significantly inhibited the release of norepinephrine (NE), a neurotransmitter that promotes macrophage migration, from adrenergic cells. In vivo, tumor tissues from 4T1 tumor-bearing mice treated with NP-BUP showed a significant reduction in NE content and macrophage infiltration, with tumor volume and weight decreasing by approximately 70% compared to the PBS group.

Conclusion: Our study provides a TME pH-responsive nanoplatform for targeted suppression of neuronal control within the TME. Our results demonstrate that specifically modulating innervation within the TME can influence the growth of breast cancer.

Keywords: pH-responsive nanoparticles, noradrenergic neurons, neuromodulation, tumor-associated macrophage, triple negative breast cancer

Introduction

Over the past decade, seminal studies have demonstrated that nerves within the tumor microenvironment (TME) can promote the malignant phenotype of tumors.[1–3] Tumors can promote the entry of nerves into the TME by secreting neurotrophic factors and axonal guidance molecules.[4] Solid tumors are innervated by different types of nerves, including sympathetic, parasympathetic, and sensory nerves. The innervation patterns and density of these nerves vary significantly depending on the type of solid tumor, reflecting the heterogeneity in tumor biology and microenvironment. In the context

Received: 5 January 2025
Accepted: 28 April 2025
Published: 12 May 2025

of breast cancer, the increased density of nerves has been proven to be an independent prognostic factor for poorer outcomes and adverse clinical outcomes.[5–7] Therefore, nerve-targeted therapeutic strategies have been proposed.

Numerous methods to eliminate neural innervation within tumor tissues have been attempted, such as surgical resection of nerve plexuses and pharmacological or genetic denervation.[8,9] However, nerve plexus resection is an invasive procedure that inevitably causes pain and tissue damage.[10] Due to the inherent non-specificity of targets, pharmacological denervation methods may lead to adverse reactions.[11,12] For instance, the beta-adrenergic receptor blocker propranolol, which can block adrenergic neural signals, may carry the risk of side effects related to the central nervous and respiratory systems when administered systemically (such as sleep disturbances, agitation, bronchospasm/bronchial hyperresponsiveness, and hypoglycemia).[13]

Bupivacaine is a commonly used local anesthetic that works by binding to the intracellular domain of voltage-gated Na^+ channels to prevent depolarization of peripheral nerves.[14] It is primarily administered around the nerves or intrathecally to block the nerves of a specific part of the body.[15] It exerts blockade effect on all major peripheral nerve subtypes, including sympathetic, parasympathetic, sensory, and motor fibers. This broad-spectrum neural blocking property makes bupivacaine not only an effective analgesic but also a potential therapeutic agent for modulating various neural signaling pathways. Given its pharmacological characteristics, it can be used to block the innervation of tumor sites.[16] However, The nerve-blocking effect of a single injection of bupivacaine typically lasts for a few hours, with a half-life of approximately 2 to 6 hours. This duration is insufficient to meet the long-term nerve block requirements.[17] Moreover, dense tumor tissue and increased interstitial fluid pressure form physiological barriers to the diffusion of local anesthetics.[18,19] Therefore, there is an urgent need to take some measures to achieve long-lasting nerve blockade by local anesthetics. Encapsulating bupivacaine into nanoparticles seems to be a promising approach. A substantial amount of research has proven that nanomedicine has emerged as a key solution for optimizing drug penetration and accumulation in tumor tissues.[20–22] The long-term nerve-blocking effect of bupivacaine nanoparticles has been extensively demonstrated and practiced in the field of pain research. Numerous studies have successfully utilized bupivacaine nanoparticles to achieve prolonged analgesia through sustained nerve blockade.[23,24] Notably, advancements in this field have led to commercialized products, such as the bupivacaine liposome formulation EXPAREL.

To achieve long-lasting nerve blockade in the TME, in addition to extended-release, the stimulus-responsive drug release pattern at the tumor site is also crucial. Among the array of stimulus-responsive materials, pH-responsive materials are widely applied due to the characteristically acidic extracellular pH (6.5–7.0) of tumors, a consequence of their aberrant metabolic processes compared to healthy tissues.[25–28] In this investigation, we employ a nanoplatform constructed from an acid-responsive copolymer. This copolymer is synthesized by covalently linking polyethylene glycol (PEG) and polylactic-co-glycolic acid (PLGA) segments through a tumor-acidity-cleavable amide bond.[29,30] Upon extravasation into the TME, the pH-sensitive amide bond undergoes hydrolysis, triggering the detachment of the PEG shell. This event facilitates the enhanced cellular internalization of the encapsulated bupivacaine.

By employing this nanoplatform, we can investigate the influence of nerve on tumor growth and to elucidate the mechanisms involved. Extensive literature has established that tumor-associated macrophages (TAMs), which are one of the most prevalent immune cell types in many solid tumors, can promote oncogenic processes by secreting growth factors that contribute to tumor development and by producing proteins and proteolytic enzymes that facilitate tumor invasion and metastasis.[31,32] It is indicated that TAMs express abundant neurotransmitter receptors on their surface, rendering them sensitive to neural signaling. Recent studies have highlighted the intricate relationship between TAMs and the nervous system, revealing that neural components can interact with these immune cells to modulate tumor behavior.[33,34] The modulation of TAMs through neuroimmune signaling pathways presents a promising avenue for therapeutic intervention. Therefore, in this study, we explore the effect of innervation on TAMs infiltration and tumor growth through nerve blockade in the TME by the acidic TME-responsive nanoparticles loaded with bupivacaine. We anticipate that our findings will contribute to the foundation of nerve-based tumor therapeutic strategies.

Materials and Methods

Materials and Reagents

Meo-PEG_{5k}-$Dlink_m$-$PLGA_{11k}$ copolymer was purchased from Xi'an Ruixi Biological Technology Co., Ltd (Xi'an, China). Norepinephrine (N72070) and bupivacaine (B92400) were acquired from Acmec (Shanghai, China).

ICI118,551 (HY-13951) was obtained from MedChemExpress. Rat anti-F4/80 antibody (ab6640) was purchased from Abcam. Dylight 594-conjugated secondary antibody (E032440) was acquired from Earthox (Burlingame, USA). Anti-CD16/CD32 antibody (clone 2.4G2), anti-CD45 antibody (clone 30-F11), anti-CD11b antibody (clone M1-70) and anti-F4/80 (clone T45-2342) were purchased from BD biosciences, USA. Ki67 antibody was obtained from Wuhan Servicebio technology CO., Ltd (Wuhan, China). (1,1'-dioctadecyl-3,3,3',3'-tetramethylindodicarbocyanine perchlorate (DiD, D307) was purchased from Thermofisher, USA. Organic solvents (DMF, DMSO and 75% ethanol) were purchased from Sigma-Aldrich and were used directly. Water was prepared using a Milli-Q system (Millipore®, Bedford, MA, USA). Transwell insert 8.0 μm were purchased from Corning (New York, USA). NE High sensitive ELISA kits (BA E-5200R, LDN, Germany) and Fluo-4 calcium detection kit (S1061, Beyotime, China) were used according to manufacturer's protocol.

Preparation and Characterization of Bupivacaine-Loaded TME pH-Responsive Nanoparticles

The nanoprecipitation method was used to prepare bupivacaine-loaded nanoparticles (NP-BUP). Briefly, Meo-PEG-Dlink$_m$-PLGA polymer and bupivacaine were dissolved in DMF separately to form homogeneous solutions with a concentration of 20 mg/mL. Subsequently, a mixture of bupivacaine solution and 200 μL Meo-PEG-Dlink$_m$-PLGA polymer solution was prepared and added in a dropwise fashion to 5 mL of deionized water while vigorously stirring (1200 rpm). The resulting solution was then transferred to a dialysis tube (EMD Milipore, MWCO 100k) for purification via centrifugation (Eppendorf, 2800 rpm × 10 min, repeated 3 times) to obtain nanoparticles (NPs). Five different bupivacaine-loaded NPs (denoted NP-BUP20, NP-BUP30, NP-BUP50, NP-BUP100, NP-BUP200) were prepared and their feed composition is shown in Table S1.

The molecular structure of bupivacaine prevents it from binding to fluorochromes. Therefore, we opted to utilize fluorescein DiD as a substitute to prepare NP-DiD for the purpose of tracking their distribution. Similarly, we use DMF as a substitute for bupivacaine to synthesize NP-control as a negative control.

Dynamic light scattering (DLS, Malvern Zetasizer) was used to examine the size and zeta potential of NPs. The morphology of NP-BUP was visualized using transmission electron microscopy (TEM; FEI Tecnai G2 12, Eindhoven, Netherlands).

Encapsulation Efficiency of Bupivacaine in NPs

Bupivacaine concentration standard curve was determined by using an ultraviole tspectrophotometer (EVOLUTION201, Thermo Scientific, USA) equipped with matching quartz cells at a resolution of 1 nm from 250 nm to 350 nm. To examine encapsulation efficiency (EE) of bupivacaine, the filtrates obtained from the three centrifugation cycles were gathered. The free bupivacaine concentration in the filtrates was calculated by comparing the absorbance value at 262nm to bupivacaine standard curve. EE (bupivacaine) was calculated as: EE = (B1 − B2)/B1×100%, where B1 and B2 are the masses of the initially added bupivacaine and non-encapsulated bupivacaine in filtrates, respectively. Concurrently, EE (bupivacaine) in NP-BUP was further determined by high performance liquid chromatography (HPLC). The HPLC test conditions were as follows: the chromatographic column was C18 (4.6 × 250 mm, 5 μm), the mobile phase was methanol: acetonitrile: 0.1% trichloroacetic acid aqueous solution =60:20:20, and the flow rate was 1.0 mL/min. EE (bupivacaine) was calculated as: EE =amount of bupivacaine in NP-BUP/total amount of bupivacaine added for NP preparation) × 100%.

In vitro Release Profile

NP-DiD (n = 3) was prepared as described above and dispersed in 1 mL of PBS (pH = 7.4). The PBS suspension of NP-DiD was transferred to a Spectra-Por® Float-A-Lyzer® G2 dialysis device (1mL, MWCO 100kDa, USA) and subsequently immersed in 1 L of PBS (pH 7.4 or 6.5) at 37°C. At predetermined intervals (5 min, 10 min, 15 min, 30 min, 1h, 2h, 4h, 8h, 24h), 10 μL NP-DiD suspension was withdrawn from the interior of the dialysis device and mixed with 200 μL DMSO. After thoroughly mixed, the fluorescence intensity of DiD was measured using a multimode microplate

reader (BioTek Synergy H1, Winooski, VT, USA). The cumulative DiD release was calculated as: Cumulative release (%) = $(F_\infty - F_t) / F_\infty \times 100\%$, where F_∞ is the fluorescence intensity of DiD encapsulated in NPs and F_t is the fluorescence intensity of DiD released from the NPs at the time point t.

Cell Culture

PC-12 and 4T1 cells were purchased from Procell Life Science & Technology Co., Ltd (CL-0481, CL-0007). The PC-12 cell line is a rat adrenal pheochromocytoma cell line commonly used for studying noradrenergic neurotransmitter. The 4T1 cell line is a highly metastatic murine breast cancer cell line used for in vivo tumor models and metastasis studies. The cells were cultivated at 37°C with 5% CO2 in DMEM and RPMI 1640 medium, respectively. The culture medium was changed every two days and 10% (v/v) fetal bovine serum (FBS) and 1% (v/v) penicillin-streptomycin solution were added. Mycoplasma contamination in cell cultures is routinely assessed using a combination of microscopy observation and PCR methods.

In vitro Cellular Uptake

PC-12 cells were seeded on poly d-lysine-coated (Sigma, P7280) glass coverslips at a density of 50,000 per coverslip. After 24h incubation, the culture medium was replaced with 500 μL fresh DMEM medium supplemented with 10% FBS at pH 7.4 or pH 6.5. Meanwhile, NP-DiD was added to culture medium and the final concentration of NP-DiD was 10nM. Following 4h of incubation at 37°C, the medium was discarded. The cells were washed with PBS three times and fixed with 4% (w/v) paraformaldehyde (PFA). To label the cell membrane, the cells were treated by 10 μg/mL Wheat Germ Agglutinin (WGA, Thermofisher, W11261) coupled to the Alexa Fluor™ 488 fluorochrome for 10 min at 37°C and then washed with 1×PBS three times. Subsequently, the nuclei were counterstained with 1 μg/mL DAPI (Sigma, D9542) for 15 min in the dark. After staining with DAPI, the coverslips were transferred to slides and mounted for imaging. Images were captured using a confocal laser microscope (Zeiss LSM 800 with Airyscan). To further qualitatively examine cellular uptake, PC-12 was seeded in 24-well plates (30,000 per well) and then the medium was exchanged with 500 μL fresh DMEM culture medium supplemented with 10% FBS containing 1nM NP-DiD at pH 7.4 or 6.5, respectively. After 4h incubation, the cells were trypsinized and collected for flow cytometry quantitative analysis (BD FACSAria™III, USA).

Isolation and Culturing of Bone Marrow-Derived Macrophages

To obtain bone marrow-derived macrophages (BMDMs), freshly isolated femur and tibia from healthy female BALB/c mice aged 6–8 weeks were flushed with cold PBS to obtain bone marrow cells. The bone marrow cells were cultured in 1640 medium supplemented with 10% FBS and M-CSF (30 ng/mL) to stimulate BMDMs maturation and differentiation for seven days. The BMDMs were subsequently harvested, and their purity was assessed using flow cytometry with the BD FACSAria™ III (BD Biosciences, USA) flow cytometer.

Transwell Migration Assay

The bone marrow-derived macrophages (BMDMs) were seeded onto the upper chamber of a transwell insert (Corning, 6.4 mm diameter, 8 μm pore size), and subsequently, the insert was placed into each well of a 24-well plate, which had been pre-filled with 700 μL of culture medium containing various chemoattractants. After incubation for 24h at 37°C, the migratory cells were fixed with 4% PFA and stained with 0.2% crystal violet. The non-migratory cells were removed from the upper surface of the transwell membrane by gently scrapping with a cotton swab. All experiments were repeated at least three times. Multiple images of migratory cells were captured in a microscope and overlapped fields were avoided. ImageJ were used to automatically analyze and determine the number of migratory cells in the image.

In vitro Cytotoxicity

Cells were seeded in 96-well plates with a density of 6000 cells/well. After incubation for 24h, the medium was substituted with 100 μL of fresh medium supplemented with a predetermined concentration of bupivacaine or NP-BUP and the cells were further incubated for an additional 24h. Subsequently, 10 μL of CCK-8 solution was added to each

well, and the plates were incubated for 1 hour to assess cell viability. Measure the absorbance at 450 nm using a microplate reader. Cell viability was calculated as: Cell viability (%) = $(A_{treated} - A_{blank})/(A_{control} - A_{blank}) \times 100\%$, where $A_{treated}$ is the absorbance obtained in the presence of cells and NPs, A_{blank} is the absorbance obtained in the absence of cells and NPs and $A_{control}$ is the absorbance obtained in the absence of cells.

Enzyme-Linked Immunoabsorbent Assay

PC-12 cells were seeded either individually at a density of 10^5 cells per well or co-cultured with 4T1 cells at a ratio of 1:5 in a 6-well plate. After incubation for 24h, the medium was refreshed with either fresh medium or medium containing NPs. After a subsequent 24-hour incubation, the supernatants from each group were harvested for analysis.

Collected tumor tissues were homogenized 10% w/v in ice-cold mixture of hydrogen chloride (10 nm) in the presence of EDTA (1 nM). Homogenates were centrifugated at 14000 ×g for 20 min at 4°C, supernatants were isolated and used for a quantitative determination of NE. NE levels in supernatants were measured using NE High Sensitive ELISA kits (LDN, BA E-5200R Germany) according to the manufacturer's protocols.

Intracellular Ca^{2+} Measurement

PC-12 cells were harvested and suspended in round-bottom tubes at a concentration of 10^6 cells per tube. They were then incubated with 1 mL of Fluo-4 AM (Beyotime) in the dark at 37°C for 20 min. Subsequently, the cells were washed twice with HEPES buffer to remove any extracellular dye. The cells were gently re-suspended in assay buffer containing 1.5 mm $CaCl_2$ and allowed to equilibrate in an incubator for 20 minutes. After a brief recording of baseline fluorescence intensity (FI) at 488 nm using flow cytometry, the cells were exposed to 200 μL of 4T1 cell supernatant to monitor changes in FI. For the bupivacaine-treated groups, cells were pre-treated with 0.3 mm bupivacaine for 5 minutes before stimulation with the 4T1 cell supernatant.

Mice

Healthy female BALB/c mice (6–8 weeks old) were obtained from Experimental Animal Center of Sun Yat-sen University and were maintained at 5 animals per cage under specific pathogen-free condition with free access to water and food in an environment maintained at approximately 22°C. All in vivo experiments were conducted in compliance with the ethical guidelines established by the National Institutes of Health for the care and use of laboratory animals. All animal experiments were approved by Institutional Animal Care and Use Committee of Sun Yat-sen University (SYSU-IACUC-2023-000095).

Pharmacokinetics

Healthy female BALB/c mice were randomly divided into two groups (n = 3) and intravenously injected with either free DiD or NP-DiD (0.35 mg DiD per kilogram of body weight), respectively. At predetermined time points, 20 μL of blood was withdrawn from the retroorbital plexus and mixed with 200 μL deionized water. The fluorescence intensity of DiD in the mixture was determined using a multifunctional microplate reader (BioTek Synergy H1, USA).

Construction of Triple Negative Breast Cancer Xenograft Model

Triple negative breast cancer xenograft model was established by subcutaneous injection with 100 μL of 4T1 cell suspension (1×10^7 cells/mL, a mixture of DMEM medium and Matrigel in 1/1 volumetric ratio) into the second pair of mammary fat pads of healthy female BALB/c mice (6~8 weeks). When the tumor volume size reached ~100mm^3, the mice were randomized and used for the following in vivo experiments.

Biodistribution

4T1 tumor-bearing mice were randomly assigned into two groups (n=3) for an intravenous injection of either (i) free DiD (0.35 mg/kg) or (ii) NPs-DiD (0.35 mg/kg equivalent dose of DiD). Twenty-four hours subsequent to the injection, the entire mouse images were observed by an IVIS Lumina III (PerkinElmer) imagine system.

Inhibition of Tumor Growth

4T1 tumor-bearing mice were randomly divided into four groups (n = 5): PBS group, NP-control group, BUP group and NP-BUP group. Specifically, the PBS group, NP-control group and NP-BUP group were administered intravenous injections of PBS, empty NPs and bupivacaine-loaded NPs (5 mg/kg bupivacaine equivalent dose). The BUP group received a direct injection of 5 mg/kg bupivacaine adjacent to the tumor site. The mice were injected once every two days for a total of 4 times. Tumor growth was monitored every two days by measuring the perpendicular diameter of the tumors using a Vernier Caliper and tumor volumes were calculated as the following equation: $V = W^2 \times L/2$, where W and L are the shortest and longest diameters, respectively.

Flow Cytometry

After the aforementioned treatment by (i) PBS, (ii) NP-control, (iii) free BUP or (iv) NP-BUP, mice were sacrificed and tumors were collected, minced and digested for 40 min in collagenase IV (Worthington-biochem, LS004186) and DNAse I (Worthington-biochem, LS002138) before being mashed through a 70 μm cell strainer. RBC lysis buffer (Beyotime, C3702) was used to lysis RBCs. After washing with PBS thrice, cells were gently re-suspended and blocked by CD16/CD32 antibody for 5 min at 4°C to minimize non-specific binding. Then the cells were stained by cell surface marker CD45, CD11b and F4/80 for 30 min in darkness at 4°C. The cells were then washed and re-suspended for FACS assay. TAMs were identified as $CD45^+$, $CD11b^+$ and $F4/80^+$ live cells.

Immunofluorescence Staining

4T1 orthotopic tumor-bearing BALB/c mice were sacrificed. Tumors were harvested and prepared as paraffin-embedded sections for further analysis. The slices were heated at 60°C for 2h, deparaffinized with xylene and then hydrated in increasing concentrations of ethanol. Antigen retrieval was performed with citrate antigen retrieval solution (Beyotime, P0081) by heating slices in boiling temperature for 5 min. After cooling to room temperature, the slices were were blocked and permeabilized with PBS containing 10% goat serum and 0.3% Triton X-100 for 1 h. Then the slices were incubated with the following primary antibodies at 4°C overnight: F4/80 antibody (1:200, Abcam, ab6640); anti-TH antibody (1:600, Merck, AB152); anti-VAChT antibody (1:200, Novus Biologicals, NB110-74,764); anti-CGRP (1:200, Thermo Fisher Scientific, PA5-114929). After washing with PBS thrice, the slices were incubated with secondary antibodies conjugated with Dlight 594 (1:200, Earthox, E032440), or with Alexa Fluor 488, 594, or 555 (Thermo Fisher Scientific) for 2h and 1μg/mL DAPI (Sigma, D9542) for 5 min at RT in the dark. The images were viewed under a confocal laser scanning microscope (Zeiss LSM 800 with Airyscan).

Immunohistochemistry Staining

Following the aforementioned treatments with PBS or NPs, tumors and main organs were harvested and prepared as paraffin-embedded sections for further analysis. Tumors and main organs collected after the above treatment by PBS or NPs were prepared into paraffin embedded slices. After deparaffinization, hydration and antigen retrieval, slices containing tumor sections were treated with 3% H_2O_2 for 10 min to block endogenous peroxidase activity and then blocked and permeabilized in blocking buffer (1x PBS containing 10% goat serum and 0.2% Triton-100) for 1h. Then the slices were incubated with Ki67 antibody at 4°C overnight. After washing with PBS thrice, the slices were treated with HRP-linked secondary antibody for 30 min. For visualization of HRP-positive staining, slides were stained by DAB substrate kit according to the manufacturer's protocol. The slices were counterstained with hematoxylin for 5 min at RT before mounted. The expression of Ki67 was examined under an optical microscope.

Blood and Histological Analysis

Healthy female BALB/c mice were randomly divided into four groups (n = 3). Specifically, the PBS group, NP-control group and NP-BUP group received intravenous injections of PBS, empty NPs and bupivacaine-loaded NPs (5 mg/kg bupivacaine equivalent dose). The BUP group received a direct injection of 5 mg/kg bupivacaine around the second pair of mammary fat pads. The mice were injected once a day for a total of 3 injections. Attention was paid to observe whether the mice in BUP group and NP-BUP group exhibited convulsions or even cardiac arrest after injection.

Subsequently, the mice were sacrificed at 24h post the final injection for blood analysis. The blood was collected for blood assay. Simultaneously, the main organs were collected and prepared into paraffin embedded slices for hematoxylin-eosin (H&E) analysis.

Statistical Analysis

Statistical analysis was performed using Prism 9 software (GraphPad Software, United States). For the comparison of quantitative data, the normality and homogeneity of variance are first analyzed. When comparing the difference between two groups, the Student's *t*-test, unpaired *t*-test with Welch's correction or the Mann–Whitney *U*-test can be used. For multiple comparison, one-way analysis of variance (ANOVA), Welch's ANOVA or Kruskal–Wallis test can be used. $P < 0.05$ was deemed to represent a statistically significant difference.

Results

Synthesis and Characterization of NP-BUP

To precisely manipulate the neural innervation in the TME, we firstly construct TME pH-responsive nanoparticles loaded with bupivacaine, denoted as NP-BUP. This nano platform was prepared by nanoprecipitation method, and was constructed by the acid-reliable copolymer Meo-PEG-Dlink$_m$-PLGA. The amide linkage connecting the PEG and PLGA segments would be triggered to break by the characteristic tumor acidity.[29] The amphiphilic Meo-PEG-Dlink$_m$-PLGA copolymers possess the innate ability to self-assemble into core-shell structured NPs within an aqueous environment. The hydrophilic PEG blocks spontaneously form the outer corona of the micelles, while the hydrophobic PLGA blocks aggregate to create the inner core. Within this self-assembly process, the hydrophobic drug bupivacaine can be effectively encapsulated within the NPs' hydrophobic core. Figure 1 shows a schematic representation of NP-BUP. By manipulating the feed composition to change the physicochemical properties of NPs (Table S1), NPs-2 were selected as the nano platform for this study (ie, NP-BUP) due to their high loading capacity and appropriate particle size.[35,36] DLS analysis and TEM revealed that the NP-BUP exhibits a spherical morphology with an average diameter of approximately 100 nm (Figure 2A and B).

To determine the efficiency of these NPs in releasing their encapsulated payload in an acidic environment, the release profile of NP-DiD were examined in different pH conditions. As shown in Figure 2C, NP-DiD exhibited a significantly faster release rate at a TME-mimicking pH of 6.5 compared to physiological pH of 7.4. Specifically, within a 24-hour period, only 30% of DiD was released at pH 7.4, while approximately 60% of DiD was released at pH 6.5.

To determine if the nanoplatform could utilize its TME pH-responsive properties to enhance the cellular uptake of its payload, PC-12 cells were exposed to NP-DiD under pH conditions of 6.5 and 7.4. Figure 2D demonstrates that PC-12 cells incubated at pH 6.5 showed a higher level of fluorescence accumulation compared to those at pH 7.4, suggesting that a greater amount of DiD was internalized under acidic conditions.

The results of flow cytometry analysis confirmed the trend observed, with PC-12 cells demonstrating a 2.4-fold increase in NP-DiD uptake at pH 6.5 compared to pH 7.4, as depicted in Figure 2E and F. Collectively, these results

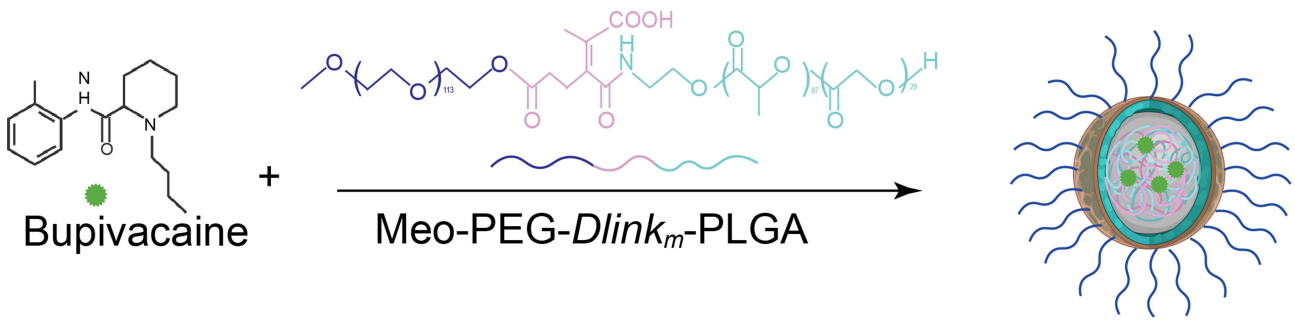

Figure 1 Schematic illustration of the synthesis of TME pH-responsive NP-BUP.

https://doi.org/10.2147/IJN.S515895

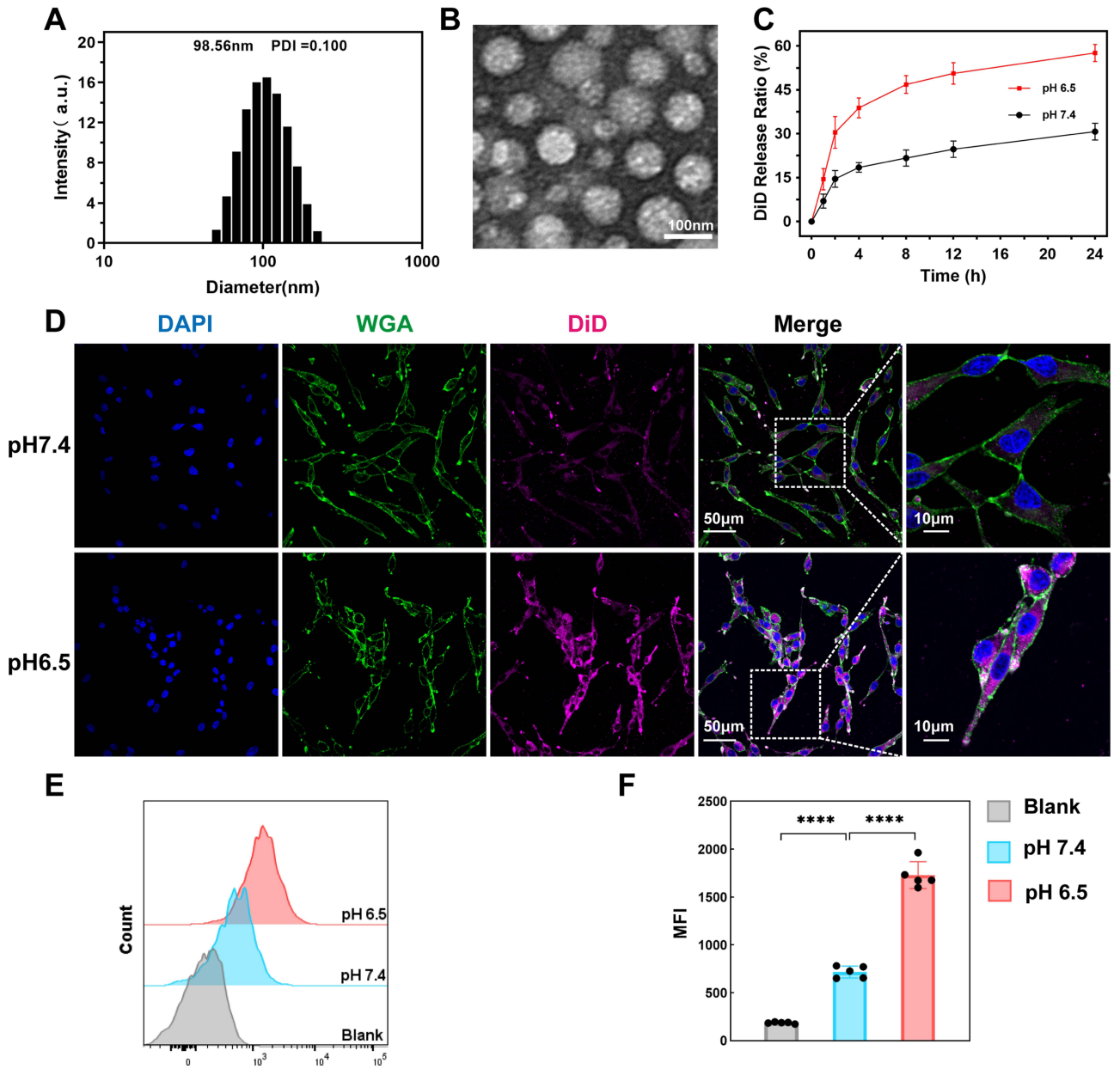

Figure 2 Characterization of NPs. (**A** and **B**) Size distribution (**A**) and TEM image (**B**) of NP-BUP in aqueous solution at pH 7.4 (**C**) Cumulative DiD release profile of NP-DiD in PBS at pH 7.4 and 6.5, respectively, mean ± SD; n = 3 (**D**) Confocal microscopy images of PC-12 cells incubated with NP-DiD at pH 7.4 and pH 6.5 for 4h, respectively. Color coding is indicated at the top. Scale bar, 50 μm. Boxes in the column (merge) are shown at a higher magnification in the latter column (scale bar, 10μm) (**E** and **F**) Representative Flow cytometry profile (**E**) and mean fluorescence intensity (MFI) (**F**) of PC-12 cells incubated with NP-DiD at pH 7.4 and pH 6.5 for 4h, respectively. n = 5. Data are mean ± SD, significant differences between treatments were calculated using One-way ANOVA followed by Tukey's post-hoc test. ****p <0.0001.

suggest that the TME pH-responsiveness of the nanoparticles at pH 6.5 can significantly enhance the cellular internalization of the encapsulated payload.

Characterization of Neuronal Type in Breast Cancer

Just as each type of tumor has its unique genetic composition and abnormalities, the nervous system that innervates the tumor region comprise different subtypes of nerves expressed at varying levels across different types of tumors.[37] In the TME, nerves may be part of the pre-existing normal neural innervation pattern of the organ or may be induced to grow into the TME by cancer cells. To explore the predominant nerve types within breast tumor tissue, we established an

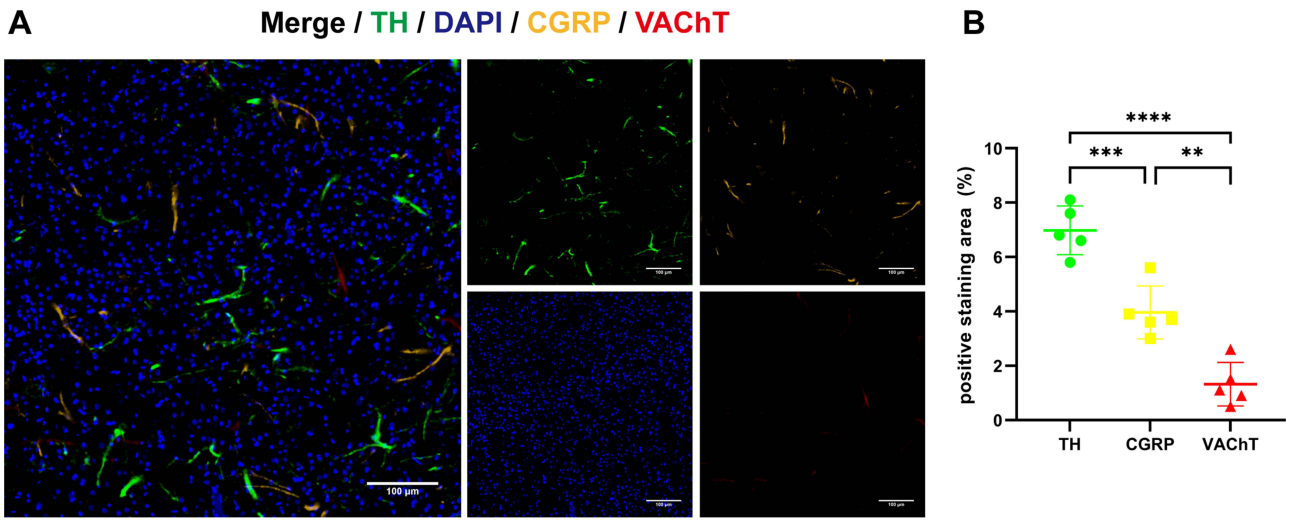

Figure 3 Evaluation of neural type in orthotopic 4T1 tumor. (**A**) Representative immunofluorescence images of tumor tissues for the adrenergic nerve marker Tyrosine Hydroxylase (TH), cholinergic nerve marker vesicular acetylcholine transporter (VAChT) and sensory nerve marker calcitonin gene-related peptide (CGRP). Color coding is indicated at the top. Scale bars, 100 μm (**B**) the quantification of TH, CGRP and VAChT density of representative images. Data show mean ± SD; significant differences were calculated using One-way ANOVA followed by Tukey's post-hoc test. **: P <0.01, ***P <0.001, ****: P <0.0001.

orthotopic 4T1 tumor-bearing BALB/c mouse model. After 3 weeks of tumor growth, the tumors were collected and subjected to immunofluorescence staining to delineate the neural distribution within the breast tumor tissue. Our results demonstrated that adrenergic nerves, marked by tyrosine hydroxylase (TH), a rate-limiting enzyme for catecholamine synthesis, had the highest density, which was significantly greater than that of cholinergic nerves (marked by vesicular acetylcholine transporter, VAChT) and sensory nerves (marked by calcitonin gene-related peptide, CGRP) (Figure 3).

Noradrenaline Enhances the Migration of BMDMs Towards Tumor Supernatant

Neuronal signals are transmitted between neurons through the exchange of neurotransmitters at synapses, and they communicate with non-neuronal cells by releasing neurotransmitters in a paracrine or endocrine manner.[38] Given our finding that noradrenergic neuronal type is the primary type of nerves in breast tumors, and based on literature reports that macrophages express a rich array of adrenergic receptors,[39] we explored the impact of NE, the principal neurotransmitter of the noradrenergic neuron, on the recruitment of macrophages by tumor supernatant. We isolated BMDMs and promoted their maturation. The purity of the macrophages was then assessed using flow cytometry. Our results demonstrated that the BMDMs exhibited a high purity level, with over 95% of cells being F4/80-positive (Figure S1). Migration assays of macrophages towards tumor supernatants with different additives revealed that the number of BMDMs migrating to the lower chamber was significantly higher in the group of 4T1 tumor supernatant containing NE compared to the group of 4T1 tumor supernatant. In contrast, there was no significant change in the number of migrated BMDMs in the group of 4T1 tumor supernatant containing the adrenergic receptor blocker ICI, or in the group of T1 tumor supernatant containing both NE and the adrenergic receptor blocker ICI (Figure 4A and D).

To evaluate the chemotactic effect of NE on BMDMs, 10 μM NE was added into the complete culture medium in the lower chamber. There was no significant difference in the number of BMDMs migrating to the lower chamber between the control group and the NE group (Figure 4B and E).

Next, to determine if NE could enhance the immune attractant ability of 4T1 cell supernatant by interacting with 4T1 cells, we preconditioned 4T1 cells with 10 μM of NE for 24 hours. Following this, the conditioned medium was replaced with fresh medium, which was then collected after an additional 24 hours and added to the lower chamber for BMDM migration assay. Concurrently, 4T1 cells in the control group were cultured in complete culture medium devoid of NE for 24 hours, followed by medium exchange and collection at the same time point as the NE-exposure group. However, no significant difference was observed in BMDMs migration between the control and NE-exposure groups (Figure 4C and F). These findings suggest that NE may enhance the recruitment of BMDMs by 4T1 cell supernatant.

https://doi.org/10.2147/IJN.S515895

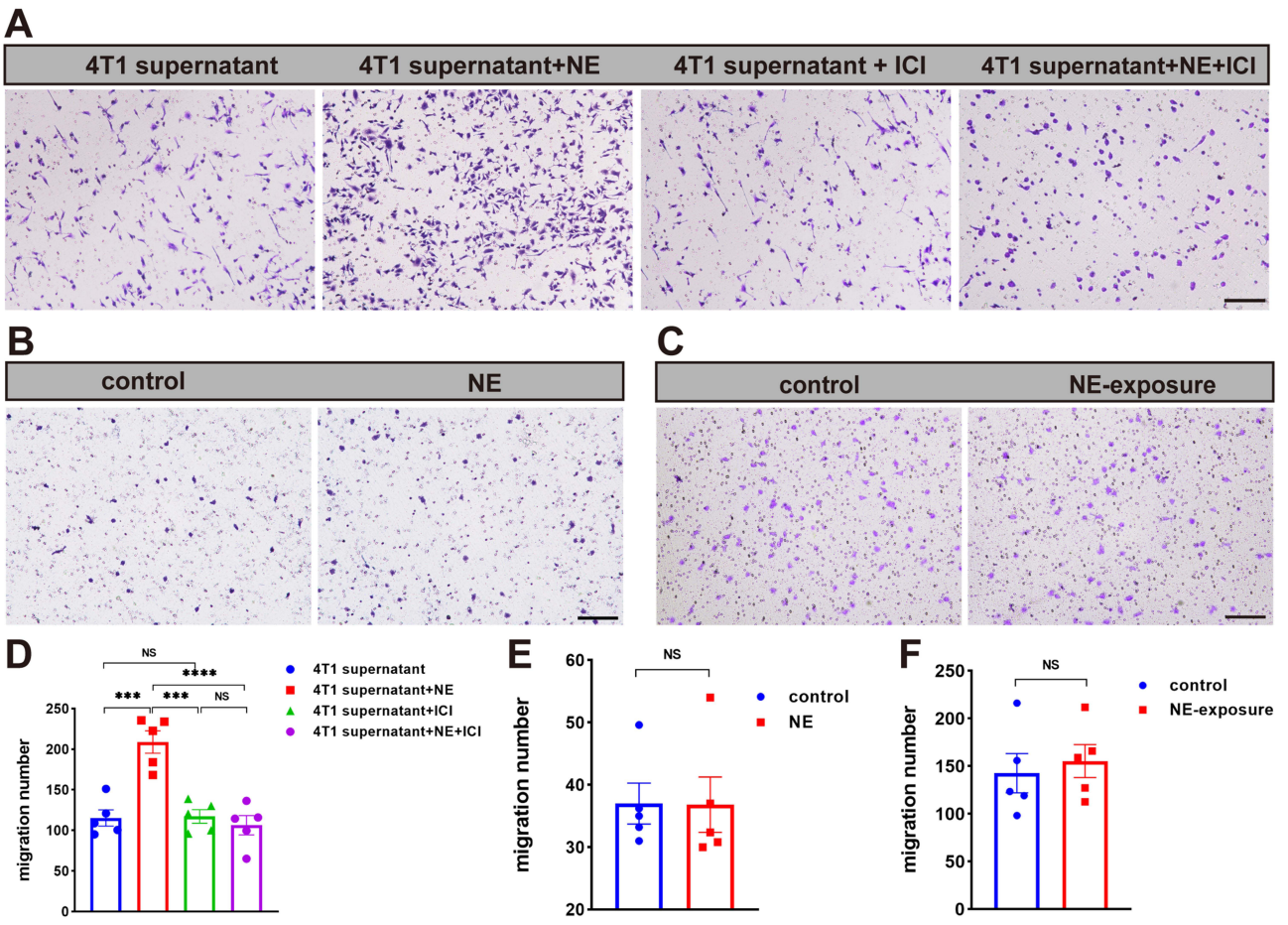

Figure 4 In vitro pro-migration effect of NE on BMDMs. (**A**) BMDMs migration assay using 4T1 cell supernatant, 4T1 cell supernatant containing norepinephrine (NE), 4T1 cells supernatant containing ICI and 4T1 cell supernatant containing NE and ICI. Scale bar, 200 μm. (**B**) BMDMs migration assay using complete culture media (the control group) and complete culture media supplemented with 10μM NE (the NE group). Scale bar, 200 μm. (**C**) BMDMs migration assay using the supernatant of 4T1 cells (the control group) and the supernatant of 4T1 cells pre-treated with 10 μM NE (the NE-exposure group) for 24h. Scale bar, 200 μm. (**D**) Quantitative analysis of the cell migration numbers in (**A**) (n = 5). Data show mean + SD, significant differences between treatments were calculated using One-way ANOVA followed by Tukey's post-hoc test. (**E**) Quantitative analysis of the cell migration numbers in (**B**) (n = 5). (**F**) Quantitative analysis of the cell migration numbers in (**C**) (n = 5). NS, not significant, ***P<0.001, ****P<0.0001.

NP-BUP Inhibits the Release of Neurotransmitters From Noradrenergic Neurons in vitro

The latest reports indicate that tumors can hijack neural signals from the central nervous system to promote tumor progression.[40] Inspired by this discovery, we explored the role of 4T1 cells in the release of NE by noradrenergic neurons and the impact of NP-BUP on this process. PC-12 cells, were either cultured alone or co-cultured with 4T1 cells, and treated with NP-control or 0.1 mg/mL bupivacaine equivalent dose of NP-BUP for 24 hours before assessing NE levels in the cell supernatant. As shown in Figure 5A, the supernatant from 4T1 cells did not contain NE. Compared to the PC-12 group, the NE content was significantly higher in the co-culture group of PC-12 cells with 4T1 cells, indicating that 4T1 cells can promote the release of NE from PC-12 cells. Compared to the co-culture group of PC-12 cells and 4T1 cells, the addition of NP-BUP significantly reduced the concentration of NE in the supernatant, while the addition of NP-control had no significant effect on the concentration of NE. This suggests that NP-BUP can effectively inhibit the release of NE from PC-12 cells.

Recognizing that local anesthetics induce concentration-dependent toxicity on the nervous system,[41] we sought to determine if the decreased NE release in the PC-12+4T1+NP-BUP group was due to a reduced PC-12 cell population during NP-BUP treatment. To this end, we evaluated the effect of NP-BUP on the proliferation of PC-12 cells. Our findings indicate that free bupivacaine exerts a notably inhibitory effect on the growth of PC-12 cells, with a half

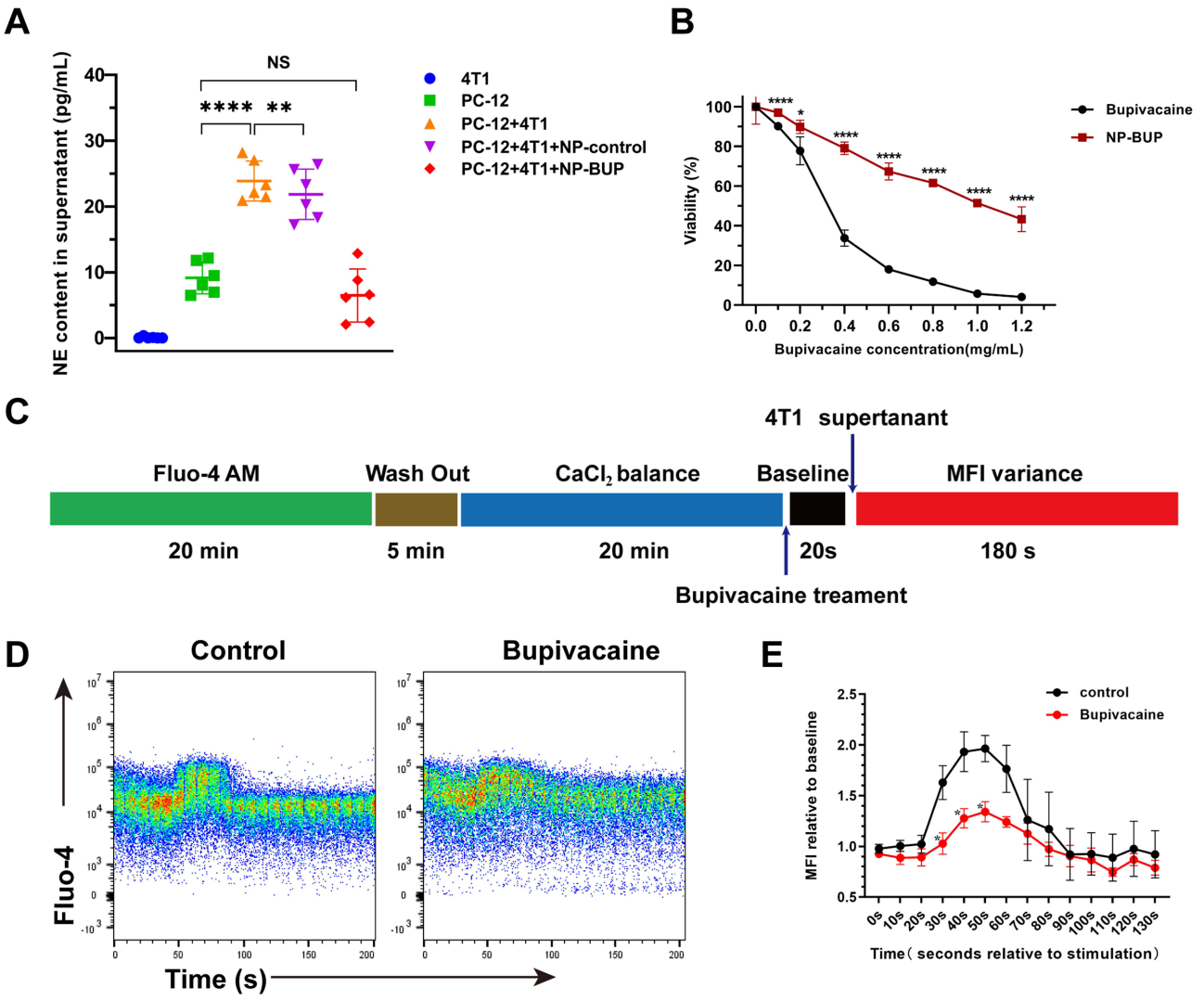

Figure 5 Bupivacaine reduced the release of NE by inhibiting the elevation of intracellular Ca^{2+} concentration in PC-12 cells. (**A**) ELISA assay of NE concentration in cell supernatant, n = 6. Significant differences between treatments were calculated using Welch ANOVA followed by Dunnett's T3 post hoc test. (**B**) Viability of PC-12 cells after treated with free bupivacaine and NP-BUP, respectively. Significant differences between treatments were calculated using Student's two-tailed, unpaired *t* test. (**C**) Schematic of protocol used to assess intracellular Ca^{2+} concentration. (**D** and **E**) Representative traces showing mean fluorescence intensity (MFI) variations of intracellular Ca^{2+} probe Fluo-4 treated by 4T1 cell supernatant in the absence or presence of bupivacaine (**D**) and mean value of MFI relative to baseline at 0s (**E**), n = 3. NS, not significant. Significant differences between treatments were determined by RM-ANOVA, followed by Mixed-effects Models for post-hoc analysis. *: *P*<0.05, **: *P*<0.01, ****: *P*<0.0001.

maximal inhibitory concentration (IC_{50}) of 0.315 mg/mL. Compared to the free bupivacaine group, the cell viability in the NP-BUP group significantly increased within the concentration range of 0.1 mg/mL to 1.2 mg/mL (Figure 5B). The IC_{50} of NP-BUP for PC-BUP cells is 1.041 mg/mL, and the cell viability remains above 95% when treated with 0.1 mg/mL bupivacaine-equivalent dose of NP-BUP. The addition of an equivalent amount of NP-control had no significant impact on the cell viability of PC-12 cells. These results suggest that 0.1 mg/mL bupivacaine-equivalent dose of NP-BUP does not significantly affect the proliferation of PC-12 cells. Therefore, the reduction in NE release observed in the ELISA experiments within the PC-12+4T1+NP-BUP group is attributed to the inhibitory effect of NP-BUP on NE release by PC-12 cells, rather than a decrease in the number of PC-12 cells.

To explore the mechanism by which NP-BUP inhibits the release of NE from PC-12 cells, we assessed the impact of NP-BUP on intracellular Ca^{2+} concentrations in PC-12 cells, as literature has reported a close association between intracellular Ca^{2+} and neurotransmitter release.[42] Initially, PC-12 cells were loaded with a Ca^{2+} fluorescence probe, which indicates intracellular Ca^{2+} concentration through mean fluorescence intensity (MFI). Flow cytometry was then employed to establish the baseline MFI of intracellular Ca^{2+} (Figure 5C). Upon the addition of 4T1 cell supernatant, there

https://doi.org/10.2147/IJN.S515895

was a significant increase in the intracellular Ca^{2+} fluorescence intensity of PC-12 cells, peaking at 202 ± 23%. This intensity gradually returned to baseline levels (Figure 5D and E). However, pre-treatment with bupivacaine prior to the addition of 4T1 cell supernatant attenuated the rise in fluorescence intensity, leading to a statistically significant decrease in the peak value (202 ± 23% vs 144 ± 11%, $P = 0.0062$). Taken together, these results demonstrate that NP-BUP can effectively suppress the release of neurotransmitters from adrenergic neurons by inhibiting the increase in intracellular Ca^{2+} concentration within the neurons.

Pharmacokinetics and in vivo Tumor-Targeting Ability of NPs

Prior to evaluating the in vivo effects of NP-BUP, we first assessed its circulation stability and its capacity to deliver payloads to tumors. As depicted in Figure 6B, free DiD was rapidly cleared from the bloodstream after injection, with only about 8% of DiD remaining detectable at 30 minutes post-injection. In contrast, NP-DiD exhibited significantly prolonged blood circulation, with approximately 10% of NP-DiD still detectable in the blood 24 hours after injection.

To exam whether this nanoplatform could efficiently delivery payloads into tumor tissues, the fluorescent dye DiD was encapsulated within nanoparticles as a tracer and administered intravenously to 4T1 tumor-bearing mice. Tumors and major organs were harvested 24 hours post-injection. As shown in Figure 6A, NP-DiD exhibited significantly enhanced accumulation in tumor tissues when compared to the free DiD group. Analysis of the fluorescence intensity in tumor tissues and collected organs revealed that the NP-DiD group had nearly four times the tumor accumulation compared to the free DiD group, which primarily accumulated in the liver and spleen rather than in tumor tissue (Figure 6C and D). These results indicate that this nanoplatform has good circulation stability and satisfactory in vivo targeting capability towards breast tumors.

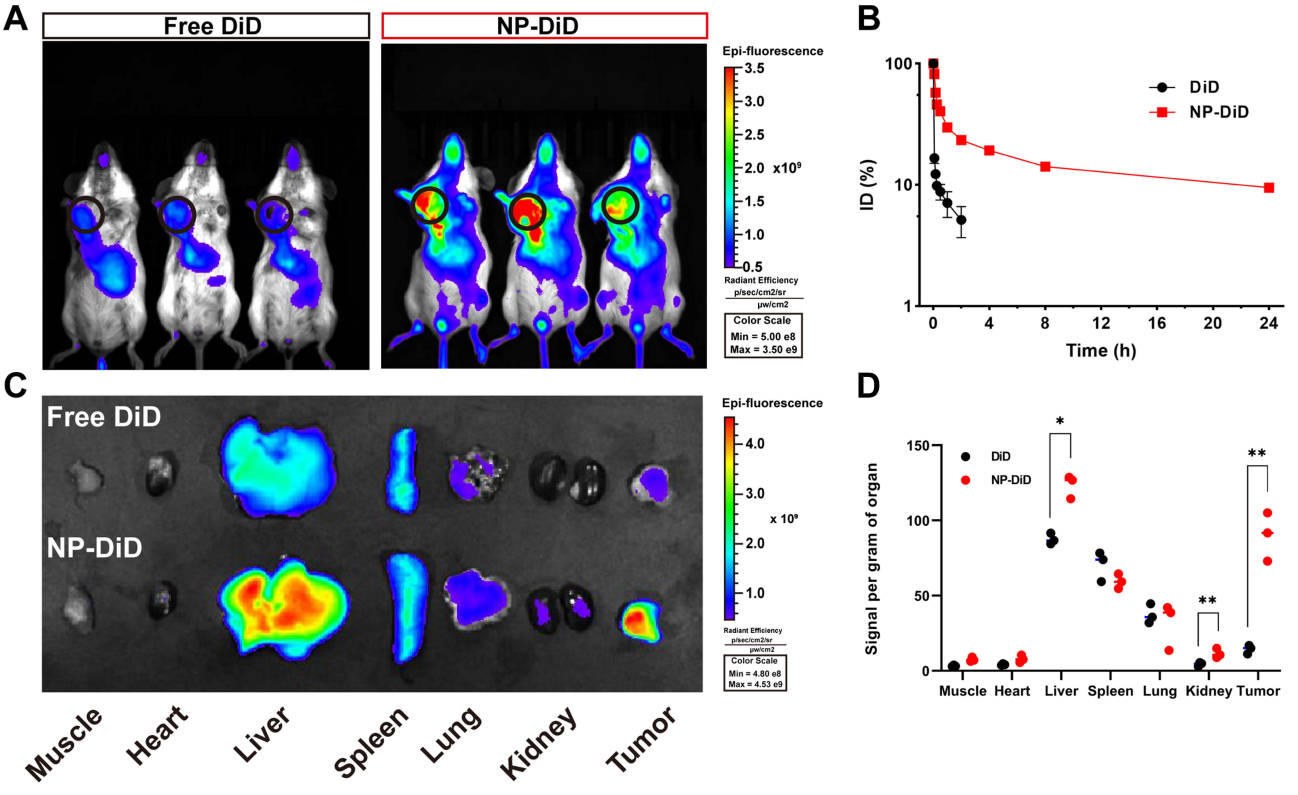

Figure 6 Pharmacokinetics and biodistribution of NPs. (**A**) Overlaid fluorescence images of 4T1 orthotopic tumor-bearing mice at 24h post inject of free DiD or NP-DiD. Tumors were indicated by ellipses. (**B**) The circulation time of free DiD and NP-DiD after intravenous injection to mice via tail vein. Mean ± SD, n = 3. (**C** and **D**) Biodistribution of DiD and NP-DiD in the tumors and major organs of 4T1 orthotopic tumor-bearing mice sacrificed at 24h post intravenous injection (**C**) and the qualification of fluorescence signal per gram organ in major organs and 4T1 orthotopic tumors (**D**). Mean ± SD, n = 3, significant differences between treatments were calculated using Student's two-tailed, unpaired *t* test. *$P < 0.05$, **$P < 0.01$ compared with free DiD group.

In vivo Suppressive Effect of NP-BUP on Noradrenergic Nerves and Macrophage Infiltration

We have demonstrated in vitro that NP-BUP can inhibit the release of NE, a neurotransmitter that promotes macrophage migration, from noradrenergic neurons. Subsequently, we further validated the impact of NP-BUP on NE levels in tumor tissues using in vivo experiments. 4T1 xenograft tumor model was employed, and when tumor volumes reached 100 mm^3, mice in each group received the corresponding treatments four times, and tumors were collected from all groups 10 days after the final treatment. According to ELISA assays, the NE content in tumors from the NP-BUP group was significantly reduced compared to the PBS group ($P<0.001$). The NE content in the NP-control group did not significantly differ from the PBS group. Although there was a trend towards decreased NE levels in the BUP group, the difference was not statistically significant compared to the PBS group. This suggests that NP-BUP is capable of inhibiting the release of NE from noradrenergic neurons within the tumor tissues.

For macrophage population analysis, viable tumor tissue samples of 0.25 g from each mouse were harvested, digested, and analyzed using flow cytometry. Cells positive for CD45, CD11b, and F4/80 were defined as tumor-associated macrophages (TAMs). Compared to the PBS group, the proportion of TAMs within $CD45^+$ cells significantly decreased in the NP-BUP group, while no significant changes were observed in the NP-control and BUP groups (Figure 7). Fluorescence staining analysis of tumor sections also supported the inhibitory effect of NP-BUP on macrophage infiltration. As shown in Figure 7, there was a noticeable reduction in F4/80-positive (red fluorescence) cells in the NP-BUP group. These findings indicate that NP-BUP is effective in diminishing the infiltration of TAMs within tumor tissues.

In vivo Antitumor Effect of NP-BUP

We ultimately assessed whether the inhibitory effects of NP-BUP on noradrenergic nerves and macrophage infiltration could translate into in vivo antitumor efficacy. As shown in Figure 8, after administering NP-BUP to 4T1 tumor-bearing mice (at a bupivacaine equivalent dosage of 5 mg/kg body weight per mouse), the growth of 4T1 tumors was significantly suppressed. Sixteen days later, the tumors volume in the PBS, BUP, and NP-control groups had grown nearly tenfold, whereas the tumors in the NP-BUP group only tripled in size. Similarly, the weight of tumors in the NP-BUP group was reduced by approximately 70%. Compared to the PBS group, the percentage of Ki67-positive cells in the NP-BUP group was also markedly decreased by about 60%. These results indicate that NP-BUP treatment exhibited good antitumor effects.

Throughout the treatment period, there was no significant loss in body weight among the 4T1 tumor-bearing mice, suggesting minimal toxicity. H&E staining revealed no damage to major organs (Figure S2), and serum biochemical tests confirmed normal liver and kidney function following NP-BUP treatment (Figure S3). These findings indicate the good biocompatibility of NP-BUP.

Discussions

Neurons within the TME play a significant role in tumor growth and dissemination.[43–45] Efforts to develop innovative anticancer therapies from a neural dimension are actively being pursued.[46] However, current clinical approaches for modulating nervous system in malignancy, such as surgical resection or pharmacological intervention, either result in pain and tissue trauma or induce central nervous or respiratory side effects.[47] In this scenario, we encapsulate bupivacaine, a commonly used local anesthetic, into intelligent nanoparticles that are TME pH-responsive, aiming to specifically inhibit neurons within the TME.

Intelligent nanoparticles are a class of nanocarriers capable of altering their physical or chemical properties in response to specific environmental stimuli, such as changes in pH or redox conditions.[48] The use of pH-responsive NPs for bupivacaine delivery is advantageous in the acidic TME (pH ~6.5–7.0), where triggered drug release enhances local specificity while minimizing systemic exposure. Existing studies demonstrate that pH-responsive NPs improve payload retention in physiological but achieve targeted release drugs in acidic tumor tissues, thereby outperforming non-responsive NPs that rely solely on passive targeting.[49,50] In our study, we utilized pH-responsive NPs featuring acid-

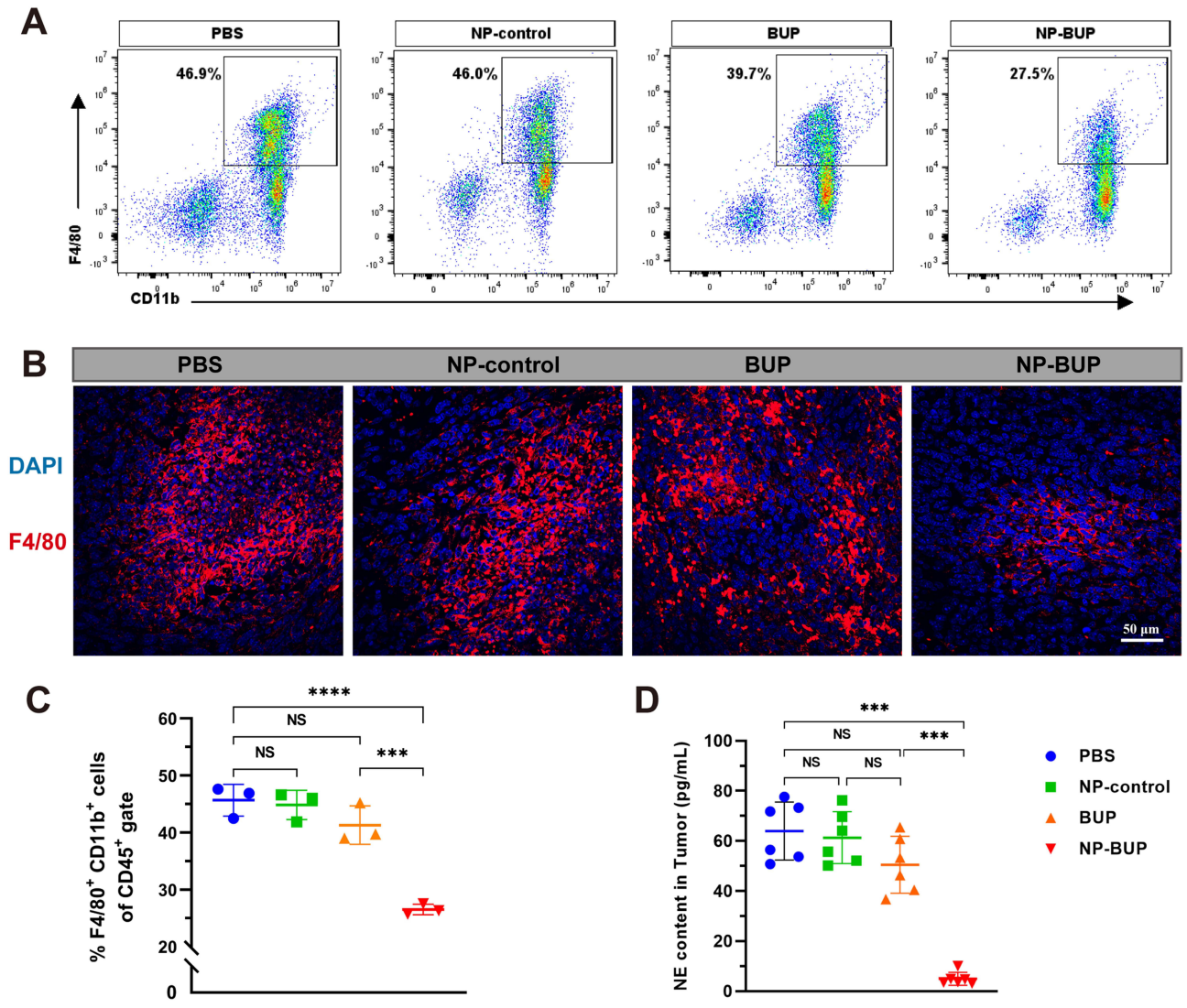

Figure 7 NP-BUP reduced the release of NE and suppressed the infiltration of TAMs in the TME of orthotopic 4T1 tumors. (**A**) Representative flow cytometry plots of TAMs in 4T1 tumors of mice treated with PBS, NP-control, BUP and NP-BUP respectively. The percentages in the graph represent the proportion of TAMs (defined as cells double-positive for F4/80 and CD11b) within the CD45-positive viable cell population. (**B**) Representative immunofluorescence images of macrophage (F4/80 staining) infiltration in 4T1 tumors treated with PBS, NP-control, BUP and NP-BUP. (**C**) Quantification of the ratio of TAMs to CD-45-positive vital cells in each group (n = 3). Significant differences between treatments were calculated using One-way ANOVA followed by Tukey's post-hoc test. (**D**) The NE contend in each group detected by ELISA assay (n=6). NS, not significant. Significant differences between treatments were calculated using Welch ANOVA followed by Dunnett's T3 post hoc test. ***$P < 0.001$, ****$P < 0.0001$.

degradable amide bonds. Upon exposure to the TME, the characteristic acidic milieu of tumors triggers the cleavage of these amide bonds, leading to the shedding of the surface PEG corona. This process promotes the uptake of drug-loaded nanoparticles by neuronal cells and facilitates site-specific targeted delivery of local anesthetics. Our data demonstrate that the uptake of nanoparticles by neuronal cells in an acidic environment (pH 6.5) is 2.4 times higher than in a normal physiological environment (pH 7.4). In vivo biodistribution study also demonstrate that the nanoparticles primarily accumulate and release at the tumor site. This is largely attributed to the enhanced permeability and retention (EPR) effect and the acid-triggered release. The bupivacaine nanoparticles we synthesized exhibit excellent TME-targeting capacity and pH responsiveness.

Neurons influence tumor growth by a complex and multifaceted method.[8,51] Given that immune cells express adrenergic receptors on their surfaces, the impact of noradrenergic neurons on immune cells within the TME has become a hot topic in the field of tumor neurology.[52,53] Recent research has revealed that sympathetic nerves can suppress the

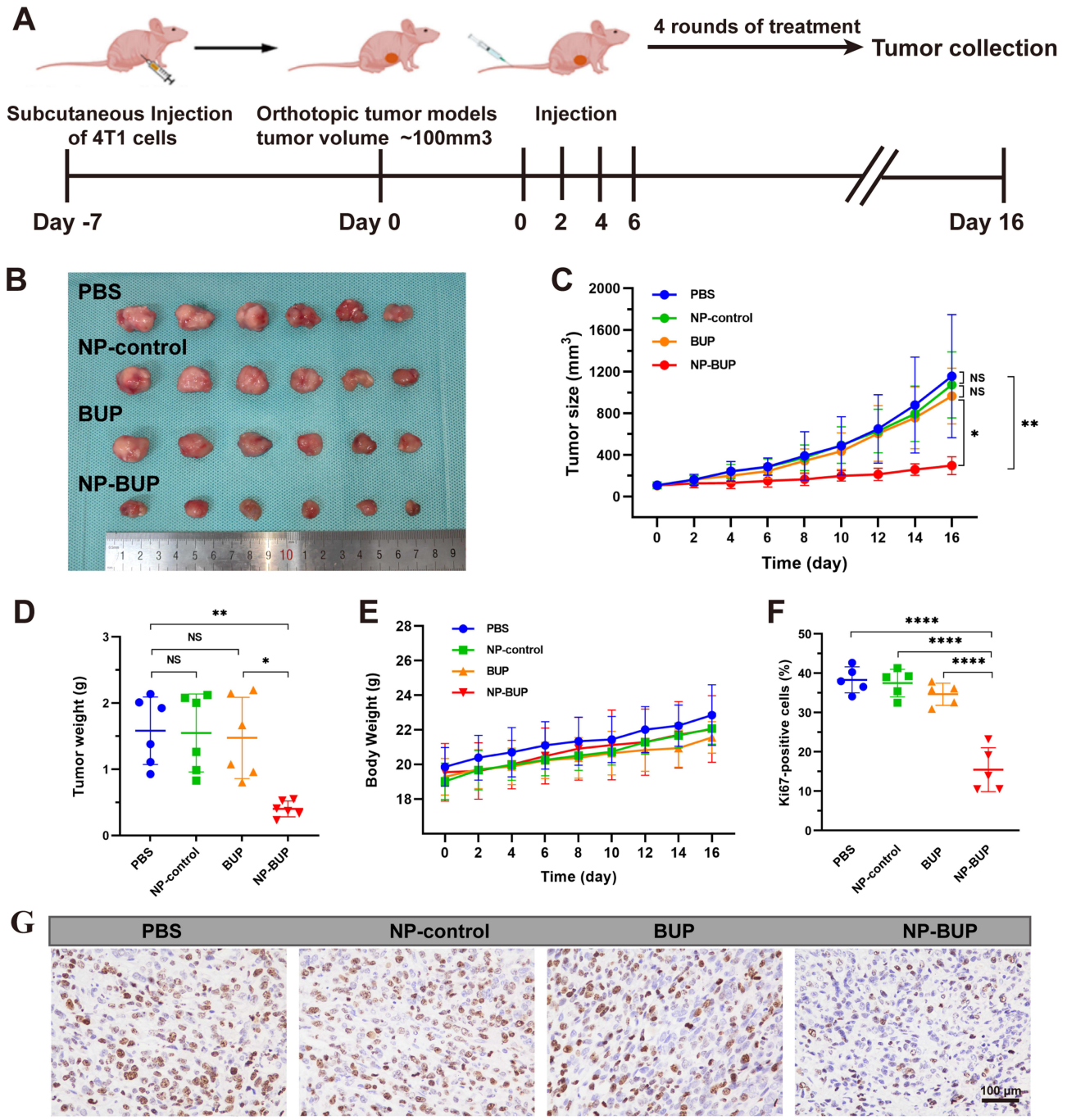

Figure 8 In vivo anti-tumor effect of NP-BUP. (**A**) Schematic illustration of 4T1 orthotopic tumor-bearing mice treated with PBS, NP-control, BUP and NP-BUP. (**B–E**) Photograph of collected tumors (**B**) tumor size (**C**) tumor weight (**D**) and the body weight (**E**) of 4T1 orthotopic tumor-bearing mice after treatment in each group. Mean ± SD, n = 6. (**F** and **G**) Ki67 staining (**G**) and quantification of proliferation (Ki67) (**F**) of 4T1 orthotopic tumor tissues after systemic treatment in each group. Mean ± SD, n =5. NS, not significant. Significant differences between treatments were calculated using One-way ANOVA followed by Tukey's post-hoc test. *$P < 0.05$, **$P < 0.01$, ****$P < 0.0001$.

secretion of cytotoxic factors TNF-α and IFN-γ from $CD8^+$ T cells in humans and rodents via adrenergic receptors on $CD8^+$ cells.[54,55] After immunofluorescence staining identified noradrenergic nerves as the primary neural types in the breast TME, we demonstrated in vitro that neurotransmitters from noradrenergic neurons promote the migration of macrophages towards tumor supernatants. The research by Kim et al further clarifies that adrenergic signaling can modify the actin structure of macrophages, transitioning from linear, unbranched filaments to branched ones, thereby enhancing the migratory function of these cells.[56] Our findings are consistent with prior work in breast cancer, which has shown that

https://doi.org/10.2147/IJN.S515895

sympathetic activation induces TAMs polarization toward an M2 phenotype and promotes macrophage accumulation in pre-metastatic lungs.[33,57,58] Our strategy of blocking sympathetic neurotransmission to suppress macrophage infiltration is in line with these mechanisms.

Building on these findings, our work introduces a novel nano-enabled approach to locally reduce noradrenergic neurotransmitter levels, thereby decreasing macrophage infiltration in the TME and inhibiting tumor growth. The mechanism behind this phenomenon is primarily because TAMs play an important supportive role in tumor growth, which can promote tumor growth through various mechanisms such as stimulating tumor angiogenesis, promoting immune suppression, and participating in metabolic reprogramming.[59,60] Therefore, when the infiltration of TAMs is reduced, tumor growth is markedly limited. This distinct mechanistic focus represents a key difference between our study and the work by Kaduri et al.[16] While both studies explore neural signaling in the TME, our research specifically investigates the crosstalk between neural and immune components within the TME and its impact on tumor progression. In contrast, Kaduri et al primarily focused on neuron-cancer cell interactions, without addressing the role of TAMs or the detailed mechanisms involving NE-mediated macrophage recruitment. Our work provides novel insights into immune-centric pathways of neural regulation in the TME. Furthermore, chemotherapy is a cornerstone of breast cancer treatment; however, the development of drug resistance and chemoresistance poses significant challenges. Recent studies have shown that chemotherapy can exacerbate sympathetic nerve infiltration into tumors, and these noradrenergic nerves are associated with chemoresistance.[37,61] These findings provide a theoretical basis for inhibiting sympathetic nerve signaling to augment chemotherapy efficacy. Our study, which investigates the use of local anesthetic nanoparticles to reduce sympathetic signaling in breast tumors, aligns with this concept, suggesting that they may become a tool in the field of breast cancer treatment.

This study has several limitations that warrant further exploration. Firstly, the research is primarily focused on triple-negative breast cancer, which may limit the generalizability of the findings to other types of tumors. Secondly, while the study has concentrated on the effects of noradrenergic neurotransmitters on the quantity of TAMs in the TME, the impact

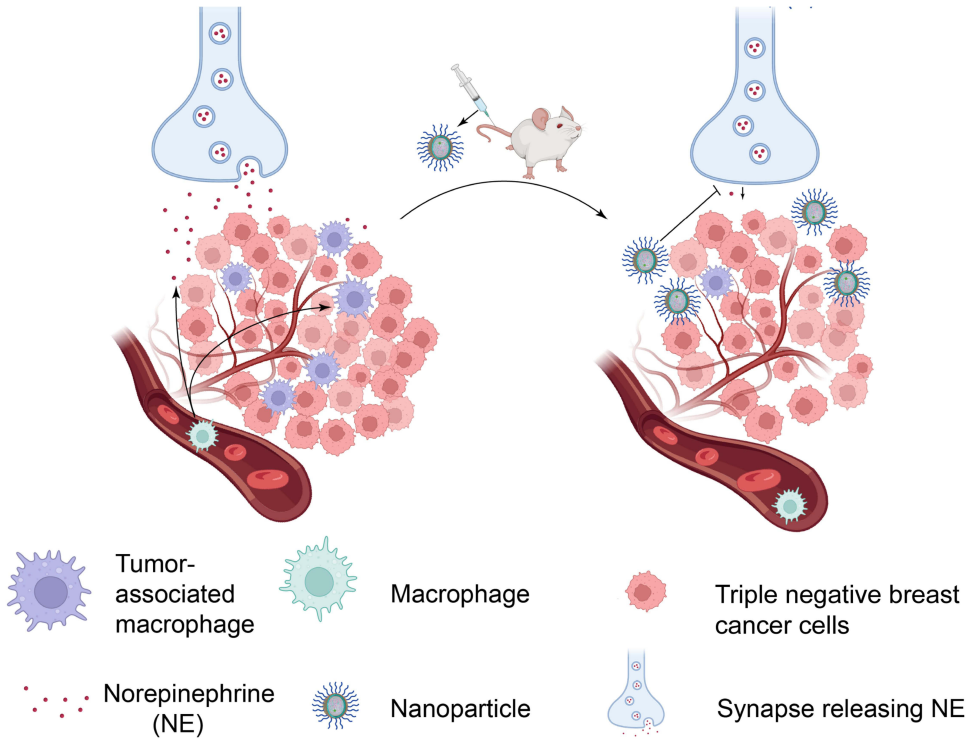

Figure 9 Schematic illustration of TME pH-responsive naoparticle NP-BUP for the targeted blockade of nerves in TME, reduction of TAMs infiltration and ultimately the suppression of tumor progression. Following intravenous injection, NP-BUP can extravasate from the leaky tumor vasculature and accumulate in the TME. Due to its TME pH-triggered release properties, the encapsulated bupivacaine within NP-BUP is released to efficiently suppress sympathetic nerves in the TME. This inhibition of nerve activity reduces the release of the neurotransmitter norepinephrine (NE), thereby decreasing TAMs infiltration and leading to significant inhibition of breast tumor growth.

on their functionality remains unassessed, and this requires further investigation in future studies. Thirdly, while our current study employed NP-DiD to preliminarily explore the biodistribution of NPs, the in vivo pharmacokinetic profiling of free BUP (released from BUP-NPs) across tumor versus normal tissues remains to be empirically quantified in future studies, which could further confirm the spatial specificity of our NP design.

In summary, we have constructed a pH-responsive nanoparticle, NP-BUP, loaded with bupivacaine. Our experimental results demonstrate that this nanoparticle exhibits good pH responsiveness, tumor targeting, and biocompatibility. When applied to 4T1 tumor-bearing mice, NP-BUP significantly reduced the concentration of noradrenergic neurotransmitters in tumor tissues, leading to a decrease in the infiltration of TAMs and ultimately inhibiting tumor growth.

Conclusion

In summary, this study reported the construction of pH-responsive nanoparticle capable of delivering bupivacaine into tumor tissues to specifically modulate noradrenergic signaling within the TME. Our findings demonstrated that targeted depletion of the neurotransmitter NE in TME could significantly reduce macrophage infiltration and ultimately successfully suppress tumor growth (Figure 9).

Funding

This work was supported by the Natural Science Foundation of Guangdong Province (No. 2022A1515010612) and the Science and Technology Projects in Guangzhou [grant number 2023A04J2102].

Disclosure

The authors report no conflicts of interest in this work.

References

1. Zahalka AH, Arnal-Estapé A, Maryanovich M, et al. Adrenergic nerves activate an angio-metabolic switch in prostate cancer. *Science*. 2017;358 (6361):321–326. doi:10.1126/science.aah5072
2. Yaman I, Çobanoğlu D A, Xie T, Ye Y, Amit M. Advances in understanding cancer-associated neurogenesis and its implications on the neuroimmune axis in cancer. *Pharmacol Ther*. 2022;239:108199. doi:10.1016/j.pharmthera.2022.108199
3. Conceição F, Sousa DM, Loessberg-Zahl J, et al. A metastasis-on-a-chip approach to explore the sympathetic modulation of breast cancer bone metastasis. *Mater Today Bio*. 2022;13:100219. doi:10.1016/j.mtbio.2022.100219
4. Magnon C, Hondermarck H. The neural addiction of cancer. *Nat Rev Cancer*. 2023;23:317–334.
5. Huang D, Su S, Cui X, et al. Nerve fibers in breast cancer tissues indicate aggressive tumor progression. *Medicine*. 2014;93(27):e172. doi:10.1097/MD.0000000000000172
6. Bjørnstad OV, Carrasco M, Finne K, et al. Global and single-cell proteomics view of the co-evolution between neural progenitors and breast cancer cells in a co-culture model. *EBioMedicine*. 2024;108:105325. doi:10.1016/j.ebiom.2024.105325
7. L D, Ln H, Sm Z, et al. High nerve density in breast cancer is associated with poor patient outcome. *FASEB Bioadv*. 2022;4:391.
8. March B, Faulkner S, Jobling P, et al. Tumour innervation and neurosignalling in prostate cancer. *Nat Rev Urol*. 2020;17(2):119–130. doi:10.1038/s41585-019-0274-3
9. Wang H, Huo R, He K, et al. Increased nerve density adversely affects outcome in colorectal cancer and denervation suppresses tumor growth. *J Transl Med*. 2025;23(1):112. doi:10.1186/s12967-025-06104-2
10. Ofosu A, Ramai D, Morgan A, Chan C, Adler DG, Siddiqui A. EUS-guided radiofrequency ablation of solid pancreatic lesions: an updated review. *Endosc Ultrasound*. 2024;13(1):1–5. doi:10.1097/eus.0000000000000036
11. Kahn M. Can we safely target the WNT pathway? *Nat Rev Drug Discov*. 2014;13(7):513–532. doi:10.1038/nrd4233
12. Zheng T, Huang J, Xiang X, et al. Systematical analysis reveals a strong cancer relevance of CREB1-regulated genes. *Cancer Cell Int*. 2021;21::1–6.
13. Hiller JG, Cole SW, Crone EM, et al. Preoperative β-Blockade with Propranolol Reduces Biomarkers of Metastasis in Breast Cancer: a Phase II Randomized Trial. *Clin Cancer Res*. 2020;26(8):1803–1811. doi:10.1158/1078-0432.CCR-19-2641
14. Skidmore RA, Patterson JD, Tomsick RS. Local anesthetics. *Dermatol Surg off Publ Am Soc Dermatol Surg Al*. 1996;22:511–522.
15. Eng HC, Ghosh SM, Chin KJ. Practical use of local anesthetics in regional anesthesia. *Curr Opin Anaesthesiol*. 2014;27(4):382–387. doi:10.1097/ACO.0000000000000091
16. Kaduri M, Sela M, Kagan S, et al. Targeting neurons in the tumor microenvironment with bupivacaine nanoparticles reduces breast cancer progression and metastases. *Sci Adv*. 2021;7(41):5435. doi:10.1126/sciadv.abj5435
17. Alejo T, Uson L, Landa G, et al. Nanogels with High Loading of Anesthetic Nanocrystals for Extended Duration of Sciatic Nerve Block. *ACS Appl Mater Interfaces*. 2021;13(15):17220–17235. doi:10.1021/acsami.1c00894
18. Blanco E, Shen H, Ferrari M. Principles of nanoparticle design for overcoming biological barriers to drug delivery. *Nat Biotechnol*. 2015;33 (9):941–951. doi:10.1038/nbt.3330
19. Zhou H, Fan Z, Deng J, et al. Hyaluronidase Embedded in Nanocarrier PEG Shell for Enhanced Tumor Penetration and Highly Efficient Antitumor Efficacy. *Nano Lett*. 2016;16(5):3268–3277. doi:10.1021/acs.nanolett.6b00820

20. Shen X, Pan D, Gong Q, Gu Z, Luo K. Enhancing drug penetration in solid tumors via nanomedicine: evaluation models, strategies and perspectives. *Bioact Mater*. 2023;32:445–472. doi:10.1016/j.bioactmat.2023.10.017
21. Li Y-J, Wu J-Y, Hu X-B, Ding T, Tang T, Xiang D-X. Biomimetic Liposome with Surface-Bound Elastase for Enhanced Tumor Penetration and Chemo-Immumotherapy. *Adv Healthc Mater*. 2021;10(19):e2100794. doi:10.1002/adhm.202100794
22. Barattin M, Mattarei A, Balasso A, et al. pH-Controlled Liposomes for Enhanced Cell Penetration in Tumor Environment. *ACS Appl Mater Interfaces*. 2018;10(21):17646–17661. doi:10.1021/acsami.8b03469
23. He Y, Qin L, Huang Y, Ma C. Advances of Nano-Structured Extended-Release Local Anesthetics. *Nanoscale Res Lett*. 2020;15(1):13. doi:10.1186/s11671-019-3241-2
24. Liu J, Wu W, Peng F, et al. Size control of ropivacaine nano/micro-particles by soft-coating with peptide nanosheets for long-acting analgesia. *Theranostics*. 2024;14(6):2637–2655. doi:10.7150/thno.93322
25. Es L, Kt O, K D, Ys Y, Yh B. Tumor pH-responsive flower-like micelles of poly(L-lactic acid)-b-poly(ethylene glycol)-b-poly(L-histidine). *J Control Release*. 2007;123:123. doi:10.1016/j.jconrel.2007.07.015
26. Lee ES, Na K, Bae YH. Super pH-sensitive multifunctional polymeric micelle. *Nano Lett*. 2005;5(2):325–329. doi:10.1021/nl0479987
27. Du J-Z, Li H-J, Wang J. Tumor-Acidity-Cleavable Maleic Acid Amide (TACMAA): a Powerful Tool for Designing Smart Nanoparticles To Overcome Delivery Barriers in Cancer Nanomedicine. *Acc Chem Res*. 2018;51(11):2848–2856. doi:10.1021/acs.accounts.8b00195
28. Prasad A, Nair R, Bhatavdekar O, et al. Transport-driven engineering of liposomes for delivery of α-particle radiotherapy to solid tumors: effect on inhibition of tumor progression and onset delay of spontaneous metastases. *Eur J Nucl Med Mol Imaging*. 2021;48(13):4246–4258. doi:10.1007/s00259-021-05406-z
29. Sun C-Y, Liu Y, Du J-Z, Cao Z-T, Xu C-F, Wang J. Facile Generation of Tumor-pH-Labile Linkage-Bridged Block Copolymers for Chemotherapeutic Delivery. *Angew Chem Int Ed Engl*. 2016;55(3):1010–1014. doi:10.1002/anie.201509507
30. Dong Z, Huang Z, Li S, et al. Nanoparticles (NPs)-mediated systemic mRNA delivery to reverse trastuzumab resistance for effective breast cancer therapy. *Acta Pharm Sin B*. 2023;13(3):955–966. doi:10.1016/j.apsb.2022.09.021
31. Christofides A, Strauss L, Yeo A, Cao C, Charest A, Boussiotis VA. The complex role of tumor-infiltrating macrophages. *Nat Immunol*. 2022;23(8):1148–1156. doi:10.1038/s41590-022-01267-2
32. Sánchez-Paulete AR, Mateus-Tique J, Mollaoglu G, et al. Targeting Macrophages with CAR T Cells Delays Solid Tumor Progression and Enhances Antitumor Immunity. *Cancer Immunol Res*. 2022;10:1354–1369.
33. Sloan EK, Priceman SJ, Cox BF, et al. The sympathetic nervous system induces a metastatic switch in primary breast cancer. *Cancer Res*. 2010;70(18):7042–7052. doi:10.1158/0008-5472.CAN-10-0522
34. Le CP, Nowell CJ, Kim-Fuchs C, et al. Chronic stress in mice remodels lymph vasculature to promote tumour cell dissemination. *Nat Commun*. 2016;7(1):10634. doi:10.1038/ncomms10634
35. Shilo M, Sharon A, Baranes K, Motiei M, Lellouche J-PM, Popovtzer R. The effect of nanoparticle size on the probability to cross the blood-brain barrier: an in-vitro endothelial cell model. *J Nanobiotechnology*. 2015;13(1):19. doi:10.1186/s12951-015-0075-7
36. Sindhwani S, Syed AM, Ngai J, et al. The entry of nanoparticles into solid tumours. *Nat Mater*. 2020;19(5):566–575. doi:10.1038/s41563-019-0566-2
37. Yaniv D, Mattson B, Talbot S, Gleber-Netto FO, Amit M. Targeting the peripheral neural-tumour microenvironment for cancer therapy. *Nat Rev Drug Discov*. 2024;23(10):780–796. doi:10.1038/s41573-024-01017-z
38. Schäffer M, Beiter T, Becker HD, Hunt TK. Neuropeptides: mediators of inflammation and tissue repair? *Arch Surg Chic Ill*. 1998;133:1107–1116.
39. Noh H, Yu MR, Kim HJ, et al. Beta 2-adrenergic receptor agonists are novel regulators of macrophage activation in diabetic renal and cardiovascular complications. *Kidney Int*. 2017;92(1):101–113. doi:10.1016/j.kint.2017.02.013
40. Xu Q, Cao Y, Kong F, et al. Multiple cancer cell types release LIF and Gal3 to hijack neural signals. *Cell Res*. 2024;34(5):345–354. doi:10.1038/s41422-024-00946-z
41. Perez-Castro R, Patel S, Garavito-Aguilar ZV, et al. Cytotoxicity of local anesthetics in human neuronal cells. *Anesth Analg*. 2009;108(3):997–1007. doi:10.1213/ane.0b013e31819385e1
42. Borst JGG, Sakmann B. Calcium influx and transmitter release in a fast CNS synapse. *Nature*. 1996;383:431–434.
43. Boilly B, Faulkner S, Jobling P, Hondermarck H. Nerve Dependence: from Regeneration to Cancer. *Cancer Cell*. 2017;31(3):342–354. doi:10.1016/j.ccell.2017.02.005
44. Zhang Y, Lin C, Liu Z, et al. Cancer cells co-opt nociceptive nerves to thrive in nutrient-poor environments and upon nutrient-starvation therapies. *Cell Metab*. 2022;34(12):1999–2017. doi:10.1016/j.cmet.2022.10.012
45. Pfitzinger PL, Fangmann L, Wang K, et al. Indirect cholinergic activation slows down pancreatic cancer growth and tumor-associated inflammation. *J Exp Clin Cancer Res CR*. 2020;39(1):289. doi:10.1186/s13046-020-01796-4
46. Shi DD, Guo JA, Hoffman HI, et al. Therapeutic avenues for cancer neuroscience: translational frontiers and clinical opportunities. *Lancet Oncol*. 2022;23(2):e62–74. doi:10.1016/S1470-2045(21)00596-9
47. Li X, Yang K, Li H, Huo R. Propranolol Treatment for Infantile Hemangiomas: short-Term Adverse Effects and Follow-Up to Age Two. *BioMed Res Int*. 2019;2019:2728952. doi:10.1155/2019/2728952
48. Yue Y, Li H, Wang X, et al. Intelligent Responsive Nanoparticles with Multilevel Triggered Drug Penetration for Tumor Photochemotherapy. *ACS Appl Mater Interfaces*. 2023;15(37):44175–44185. doi:10.1021/acsami.3c06674
49. Bhattacharya S, Prajapati BG, Singh S. A critical review on the dissemination of PH and stimuli-responsive polymeric nanoparticular systems to improve drug delivery in cancer therapy. *Crit Rev Oncol Hematol*. 2023;185:103961. doi:10.1016/j.critrevonc.2023.103961
50. Shinn J, Kwon N, Lee SA, Lee Y. Smart pH-responsive nanomedicines for disease therapy. *J Pharm Investig*. 2022;52(4):427–441. doi:10.1007/s40005-022-00573-z
51. Cui Q, Jiang D, Zhang Y, Chen C. The tumor-nerve circuit in breast cancer. *Cancer Metastasis Rev*. 2023;42(2):543–574. doi:10.1007/s10555-023-10095-1
52. Dantzer R. Neuroimmune Interactions: from the Brain to the Immune System and Vice Versa. *Physiol Rev*. 2018;98(1):477–504. doi:10.1152/physrev.00039.2016
53. Sharma D, Farrar JD. Adrenergic regulation of immune cell function and inflammation. *Semin Immunopathol*. 2020;42(6):709–717. doi:10.1007/s00281-020-00829-6

54. Estrada LD, Ağaç D, Farrar JD. Sympathetic neural signaling via the β2-adrenergic receptor suppresses T-cell receptor-mediated human and mouse CD8 + T-cell effector function. *Eur J Immunol*. 2016;46(8):1948–1958. doi:10.1002/eji.201646395
55. Raju B, Haug SR, Ibrahim SO, Heyeraas KJ. Sympathectomy decreases size and invasiveness of tongue cancer in rats. *Neuroscience*. 2007;149 (3):715–725. doi:10.1016/j.neuroscience.2007.07.048
56. Kim T-H, Ly C, Christodoulides A, et al. Stress hormone signaling through β-adrenergic receptors regulates macrophage mechanotype and function. *Fed Am Soc Exp Biol*. 2019;33(3):3997–4006. doi:10.1096/fj.201801429RR
57. Chen H, Liu D, Guo L, Cheng X, Guo N, Shi M. Chronic psychological stress promotes lung metastatic colonization of circulating breast cancer cells by decorating a pre-metastatic niche through activating β-adrenergic signaling. *J Pathol*. 2018;244(1):49–60. doi:10.1002/path.4988
58. Qin J, Jin F, Li N, et al. Adrenergic receptor β2 activation by stress promotes breast cancer progression through macrophages M2 polarization in tumor microenvironment. *BMB Rep*. 2015;48(5):295–300. doi:10.5483/BMBRep.2015.48.5.008
59. Qian B-Z, Pollard JW. Macrophage diversity enhances tumor progression and metastasis. *Cell*. 2010;141(1):39–51. doi:10.1016/j.cell.2010.03.014
60. Mao Y, Keller ET, Garfield DH, Shen K, Wang J. Stromal cells in tumor microenvironment and breast cancer. *Cancer Metastasis Rev*. 2013;32 (1–2):303–315. doi:10.1007/s10555-012-9415-3
61. Zuo S, Wang Z, Jiang X, et al. Regulating tumor innervation by nanodrugs potentiates cancer immunochemotherapy and relieve chemotherapy-induced neuropathic pain. *Biomaterials*. 2024;309:122603. doi:10.1016/j.biomaterials.2024.122603